Journal of Materials Chemistry A

Accepted Manuscript

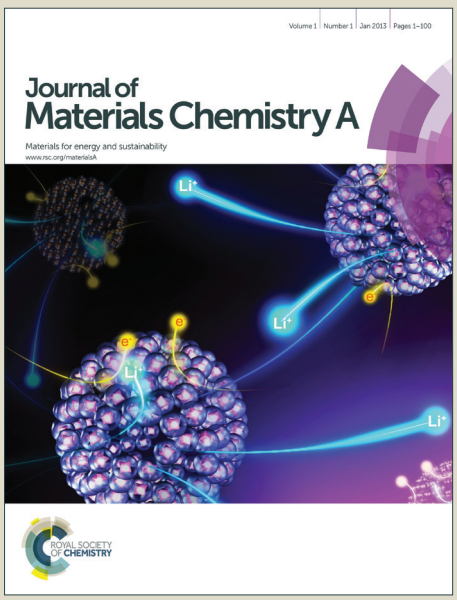

ROYAL SOCIETY OF CHEMISTRY

www.rsc.org/materialsA

Journal of Materials Chemistry A

Dynamic Article Links ►

Cite this: DOI: 10.1039/c0xx00000x

www.rsc.org/xxxxxx

Paper

Effect of Oxidation Approach on Carbon Nanotube Surface Functional Groups and Electrooxidative Filtration Performance

Guandao Gao[*a,b], Meilan Pan[a] and Chad D. Vecitis[b]

Received (in XXX, XXX) Xth XXXXXXXXX 20XX, Accepted Xth XXXXXXXXX 20XX

DOI: 10.1039/b000000x

Carbon nanotube (CNT) has found utility as an anode material for contaminant degradation; however, anode materials will inevitably undergo surface oxidation that in general has negative effects on electrochemical performance. Here, we observe that the specific CNT surface oxidation approach can preferentially form specific surface oxy-functional groups that in turn can significantly affect CNT anode performance. CNT anodes were oxidized by two methods; 1) preanodization in a sodium sulfate electrolyte (CNT-EO), to simulate electrochemical oxidation of CNT anodes, and 2) reflux in nitric acid (CNT-HNO_3) for comparison with CNT-EO. CNT characterization by XPS, FT-IR, and Boehm titration indicated that the unmodified CNT surface oxy-groups were 35.9% hydroxyl (-COH) and 64.1% carboxyl (-COOH), the CNT-EO surface groups were 47.8% -COH and 52.2% -COOH, and the CNT-HNO_3 surface groups were predominantly -COOH. As compared to an unmodified CNT anode control, the CNT-EO performance was increased by 2-fold and the CNT-HNO_3 performance was decreased by 2-fold in regards to anodic phenol mineralization and a similar trend was observed for oxalate mineralization. In agreement with the increased CNT-EO anodic performance, cyclic voltammetry and electrochemical impedance spectroscopy indicated the CNT-EO had a lower phenol electrooxidation overpotential and lower resistance to charge transfer, respectively, than both the fresh CNT and CNT-HNO_3. Thus, the specific CNT surface oxy-functional group has a strong effect on anodic performance. To further explore effect of specific CNT surface group on electrooxidation performance, experiments were also completed for the classical probe molecules of potassium ferricyanide and ascorbic acid (AA).

1. Introduction

Electrochemical oxidation kinetics of traditional bipolar electrode systems is often limited by diffusional mass transfer since convection becomes negligible within a few mm of the electrode surface. Thus, further increases in electrochemical oxidation kinetics could be made using three-dimensional porous architectures e.g., porous elemental carbon materials[1-6] such as carbon cloths and felts, where the liquid to be treated flows through the electrode increasing mass transport of the target molecule to the electrode surface for direct oxidation.[7] For example, a recently developed electrochemical carbon nanotube (CNT) filter has been shown to be effective, efficient, and rapid for the removal and oxidation of dyes and anions,[8] aromatic and aliphatic organics, [9] and bacteria and viruses.[10] However, the anode material will eventually be oxidized at potentials necessary to degrade recalcitrant pollutants.[9,11-15] In general, anode electrooxidation has adverse effects performance since surface oxidation will reduce conductivity (Ti → TiO_2) [16-18] and electrode integrity.[19, 20] The chemical/electrochemical oxidation of CNT tips and/or sidewalls has been observed to strongly affect electrochemical kinetics.[21-23] Thus, the continued development of CNT-based anodes will require an understanding of how CNT electrooxidation affects anodic performance, in particular under high potentials required for persistent contaminant degradation.

In regards to CNT electron transfer sites which are in charge of its anodic performance, the sp^2 conjugated CNT sidewalls are presumed to be mostly inactive and the edge-plane-like graphitic defect sites (i.e., open ends and tube axis defects) are assumed to be the predominant electron transfer sites.[24-26] However, a number of recent studies have questioned this hypothesis and suggest that the CNT sidewalls are also electrochemically active.[27-29] However, little work has been completed on how the specific functional group identity of the edge-plane-like graphitic defect sites, carboxyl (-COOH), carbonyl (-C=O) or hydroxyl (-COH), correlates to electrochemical activity (see table S1). Essentially, the functional groups from electrochemical or chemical oxidation of CNT should play the main role for its electrochemical performance.

Here, we examine how the specific CNT oxidation method (preanodization vs. hot nitric acid oxidation) and in turn the specific CNT surface oxy-functional group affects the efficacy and efficiency of CNT anodes towards pollutants

electrooxidation. The CNT anodes are characterized by X-ray Photoelectron Spectroscopy (XPS), Fourier Transform Infrared Spectroscopy (FT-IR), and Boehm titration to quantify the specific surface functional group. Initially, phenol and oxalate are utilized as target molecules to evaluate the effect of CNT surface oxy-group on electrochemical performance and these results are supported by phenol cyclic voltammetry (CV), electrochemical impedance spectroscopy (EIS), and LC-UV-MS product analysis. CV and EIS of the classical electrochemical probes; potassium ferricyanide ($K_3[Fe(CN)_6]$), an ideal outer-sphere redox reaction, and ascorbic acid (AA), an inner-sphere redox reaction, are also evaluated to further explore the effect of the specific CNT surface oxy-functional group on electrooxidation performance.

2. Experimental

2.1 Chemicals and Materials

Hydrochloric acid (HCl; 36.5–38.0%), nitric acid (HNO_3; 69.8%), ethyl alcohol (EtOH; ⩾ 95.0%), dimethylsulfoxide (DMSO; ⩾ 99.9%), potassium hydrogen phthalate (KHP), sodium sulfate (Na_2SO_4), sodium persulfate ($Na_2S_2O_8$), sodium bicarbonate ($NaHCO_3$), sodium carbonate (Na_2CO_3), potassium ferricyanide ($K_3Fe(CN)_6$) and ascorbic acid (AA), phenol and sodium oxalate were purchased from Sigma-Aldrich. All chemicals were purchased from Sigma-Aldrich with reagent grade except DMSO, which was spectrophotometric grade.

2.2 CNT Purification and Oxidation

The CNT were purchased from NanoTechLabs, Inc. (Yadkinville, NC) and purified (fresh-CNT) following a previously reported method to remove amorphous carbon and residual metal catalyst without oxidizing the CNT.[9] (see SI for detailed information)

The first CNT oxidation method involved preanodization (CNT-EO) of a fresh CNT network by flowing an aqueous electrolyte; $[Na_2SO_4]$ = 100 mM, pH 5.71, and $[dO_2]$ = 8 mg L^{-1}, at 1.5 mL min^{-1} through a fresh-CNT network for 4 hours at an anode potential of 1.6 V vs Ag/AgCl (1 M). The second oxidation method involved nitric acid (CNT-HNO_3) treatment of a fresh CNT sample by addition of 0.5 g CNT to 1 L of 70% HNO_3 and heating at 70 ^oC for 12 h. The oxidized CNT sample was collected by vacuum filtration onto a 5-μm pore size PTFE membrane (Omnipore; Millipore) and subsequently washed by DI water until the effluent solution was neutral pH [9].

2.3 Electrochemical CNT Filter Preparation

The CNT filters were produced by dispersing the CNT in DMSO at 0.5 mg mL^{-1} by probe sonication (Branson, Sonifier S450D) for 15 min at an applied power of 400 W L^{-1}. Then, 30-mL of the CNT-DMSO dispersion was vacuum filtered onto a 5-μm PTFE membrane (Millipore, Omnipore, JMWP). The CNT filters were subsequently washed with 100 mL EtOH, 100 mL 1:1 DI-H_2O:EtOH, and 250 mL DI-H_2O to remove any residual DMSO. Finally, the prepared filter was loaded into an electrochemistry modified filtration casing (Fig. S1). During operation, the CNT filter was utilized as the anode and was electrically connected *via* a titanium ring and wire to the DC power supply. A perforated stainless steel thin film was utilized as the cathode with an insulating silicone rubber o-ring separating the electrodes. The appropriate influent solution was then peristaltically pumped (Masterflex) through the CNT filter at the flow rate of 1.6 mL min^{-1}. Sample aliquots were collected directly from the filter casing outlet and analyzed immediately after collection as described in previous studies. [9]

2.4 Electrochemical Characterization

Electrochemical characterization of the CNT network anodes was completed with a CHI 604D (CHI Co., USA) electrochemical workstation. The prepared CNT network was employed as the working electrode, a perforated stainless steel thin film as the counter electrode, and a 1 M Ag/AgCl reference electrode utilized in a flow cell configuration with J = 1.6 mL min^{-1}. All cited potentials are referenced to 1 M Ag/AgCl unless otherwise stated. Cyclic voltammetry (CV) was performed at a scan rate of 10 mV s^{-1} and electrochemical impedance spectroscopy (EIS) was performed at 5 mV amplitude over a frequency range of 0.1-10^6 Hz.

2.5 CNT Filter Characterization

For all CNT filter samples, a survey XPS (0-1,000 eV), a C-1s (274-294 eV), and an O-1s (522-542 eV) scan were completed on an ESCA SSX-100 in Harvard's Center for Nanoscale Systems. Samples were mounted onto the sample holder with double-sided tape and loaded into the vacuum chamber via a turbo-pumped antechamber (operating pressure ≤ 5×10^{-8} Torr). The XPS data was deconvoluted using the CasaXPS 2.2 (Devon, United Kingdom). The relative atomic surface concentrations are calculated from the integrated XPS peak areas and the atomic surface concentrations of the O and C functional groups were calculated by CasaXPS. ATR-FT-IR spectra were collected using a Bruker Tensor 27 (Nankai University) over the range of 600 - 4000 cm^{-1} at a resolution of 4 cm^{-1} and the spectra were an average of 16 scans in an ambient atmosphere. A previously recorded background spectrum of water vapor and carbon dioxide was subtracted from the spectrum of each sample. Scanning electron microscopy (SEM) was completed in Harvard's Center for Nanoscale Systems on a Zeiss FESEM Supra55VP. SEM images of the filter surface and cross-section are displayed in Figure S2. Transmission electron microscopy (TEM, JEOL-2010), Brunauer−Emmett−Teller (BET) (Tristar 3000), Raman microscope (Renishaw inVia) and Contact angle (KRÜSS GmbH) was executed in Nankai University.

Boehm titration was used to determine the concentrations of the CNT surface acidic and basic functional groups.[30] Carboxyl and carbonyl and hydroxyl groups differ in their acidities and can be differentiated by neutralization with 0.01 M solutions of $NaHCO_3$, Na_2CO_3 and NaOH, respectively. Herein, three copies of 10 mg CNT-x (CNT-HCl, or CNT-EO or CNT-HNO_3) were added in 25 mL 0.01 M excess $NaHCO_3$, Na_2CO_3 and NaOH solution, respectively. Then the above solution were dispersed for 10 min by ultrasonic and stirred 6 h then filtrated. 0.01 M excess HCl were added the above filtrates, and the excess HCl were measured by the neutralization titration of 0.01 M NaOH, finally, the consumed $NaHCO_3$, Na_2CO_3 and NaOH by CNT-x can be achieved. The $NaHCO_3$ consumption and the difference between Na_2CO_3 and $NaHCO_3$ consumption as well as the difference between NaOH and Na_2CO_3 consumption, corresponds to carboxyl and carbonyl and hydroxyl groups, respectively.

2.6 Hydroxyl Radical Detection by HPLC-Fluorescence and UPLC-MS

Salicylic acid (SA) is a hydroxyl radical probe.[31] To evaluate hydroxyl radical production, an aqueous solution of [SA] = 1 mM and in [Na_2SO_4] = 10 mM was flowed through the electrochemical filter at 3.1 V cell (corresponding anode potential 1.9 V). The product of the reaction SA + HO· → Dihydroxybenzoic acid (dHBA) was quantified via high-performance liquid chromatography (HPLC) using a SB-C18 column (4.6 × 150 mm, Agilent) and a Waters 2475 Multi λ Fluorescence Detector (excitation = 314 nm; emission = 439 nm). The mobile-phase was isocratic 50/50 (v/v) MeOH/H_2O at a flow rate of 0.5 mL min^{-1}. Identification of the SA + HO· → dHBA was completed with ultra-high-performance liquid chromatography-mass spectrometry (UPLC-MS) using a UPLC column (Waters XTerra, C18 2.1×150 mm) at 40 °C, electrospray ionization (ESI) at a capillary voltage of 2.5 kV, and an ion trap mass spectrometer (Waters, Zspray) in negative ion mode over the m/z range of 50 to 300.

3. Results and Discussion

3.1 CNT Network Characterization

The fresh-CNT, CNT-EO and CNT-HNO_3 samples were characterized by XPS, FT-IR, and Boehm titration and the data is presented in Table 1 and Figure 1.

Table 1. CNT characterization from XPS, FT-IR and Boehm Titration

	XPS			FT-IR		Boehm Titration	
	O/C (%)	O1s (%)		COOH	C-OH	COOH (mmol g^{-1})	C-OH
		O-C=O	O-C				
Fresh CNTs	2.40	78.1(64.1)	**21.9(35.9)**	√	√	0.93	**0.71**
CNT-EO	3.75	68.6(52.2)	**31.4(47.8)**	√	√	1.11	**1.23**
CNT-HNO_3	3.80	~100(100)	×	√	×	1.75	**0.02**

×: not detected; √: detected peak; data in **( )** are the percentage of oxy-group O-C=O or O-C

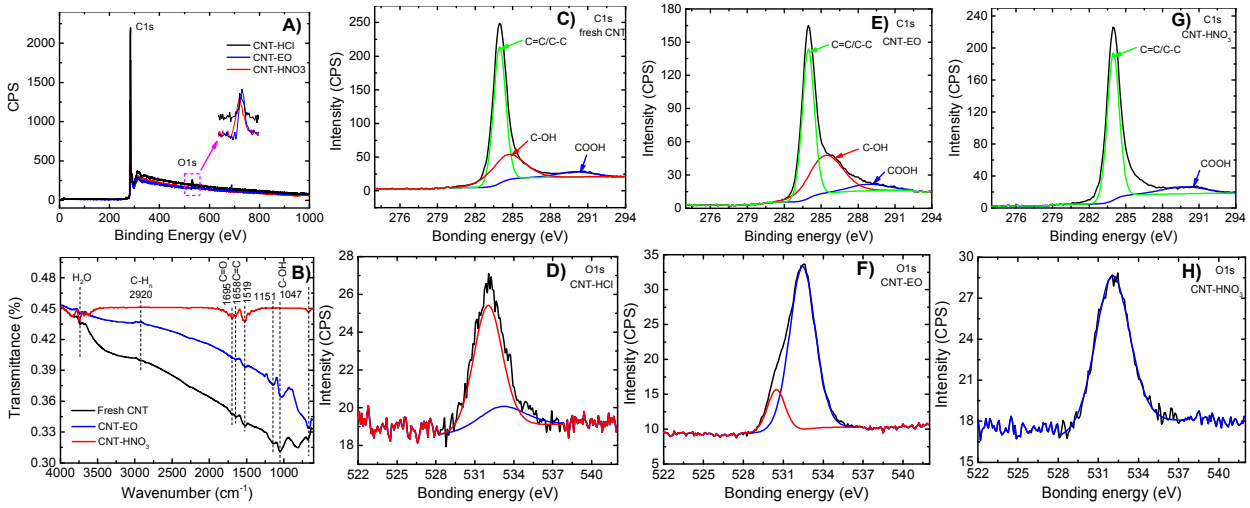

Figure 1. XPS and FT-IR spectra of the CNT samples. A) XPS full survey containing C1s and O1s; **B)** FT-IR; **C), E), G)** C1s spectra; **D), F), H)** O1s spectra.

The XPS surficial O/C ratio of the fresh CNT sample was 0.024 and increased to 0.038 for both the CNT-EO and CNT-HNO_3. An in-depth examination of the C1s and O1s specific binding energies (Figure 1 C-H and Table 1) indicates that the three samples have different specific surface oxy-functional group distributions. The fresh-CNT is mostly carboxyl (-COOH; 64.1%) with a fraction of hydroxyl (-COH; 35.9%) surface groups, the CNT-EO sample is carboxyl (-COOH; 52.2%) and hydroxyl (-COH; 47.8%) surface groups, and the CNT-HNO_3 sample is nearly 100% carboxyl (-COOH) surface groups (see SI for detail information on XPS). FT-IR was also completed on the CNT samples (Figure 1B). All CNT samples display a strong peak around 1695 and 1658 cm^{-1} attributed to the C=O (-COOH) stretching mode and the C=C stretching mode, respectively. The band at 2920 cm^{-1} is due to the asymmetric C-H_n and symmetric C-H_n stretching mode. The peak at 1047 cm^{-1} is due to C-O (COH) stretching mode[7, 32-35]. Note that the C-O (COH) stretching mode is only observed for the CNT and CNT-EO. The results here are agreement with the previous work of Wepasnick et al[36] who observed that CNT refluxed in nitric acid had a significant increase in O/C ratio and that carboxylates were the predominant surface functional group produced by this method. Boehm titration was also used to quantitatively determine oxy-functional group surface density[8]. The fresh-CNT were determined to have 0.93 mmol COOH $gCNT^{-1}$ and 0.71 mmol OH $gCNT^{-1}$, the CNT-EO had 1.11 mmol COOH $gCNT^{-1}$ and 1.23 mmol OH $gCNT^{-1}$, and the CNT-HNO_3 had 1.75 mmol -COOH/g CNT, which also agree well with the XPS analysis on CNT surface functional groups. In summary, the CNT-EO and the CNT-HNO_3 had a similar O/C ratio higher than that of the fresh-CNT and the CNT-

EO had the highest surface hydroxyl content while the CNT-HNO_3 had predominantly surface carboxylate content.

TEM and SEM images of the CNTs before and after different oxidization in Figure 2 showed that no changes in the morphology were detected in the case of non-oxidative treatment with HCl (CNT-HCl) and CNT-HCl were smooth with closed endpoint, the endpoints of CNTs were opened and the surface were eroded with the sidewall damage after electrochemical or HNO_3 oxidization.

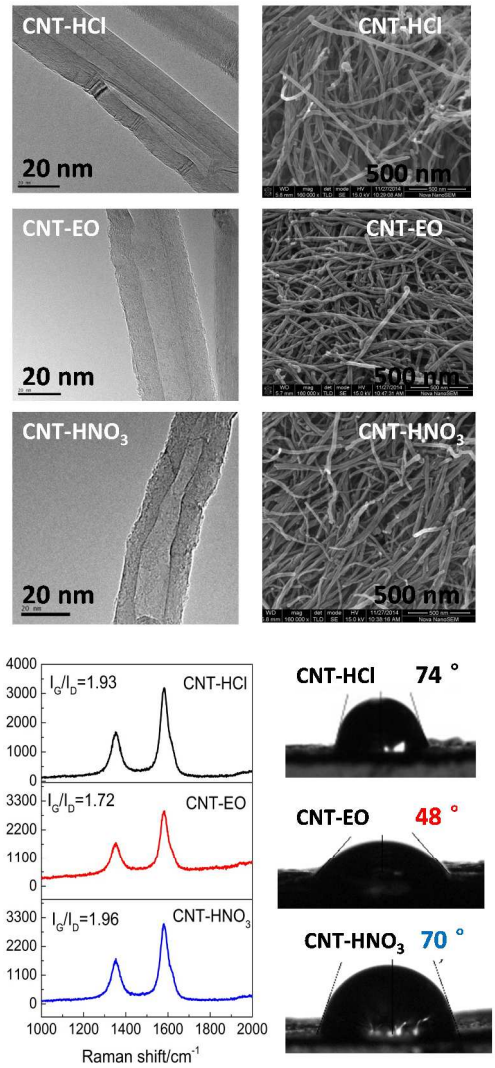

Figure 2. Images of TEM and SEM and Raman and Contact Angle of the CNT Samples.

I_G / I_D in Raman, a quantitative measure of defects density in the CNT, followed the order: CNT-EO (1.72) < CNT-HCl (1.93) < CNT-HNO3 (1.96), which meant that CNT-EO had more defects compared to CNT-HCl and CNT-HNO_3. CNT-EO surface (contact angle, 48 °) are more hydrophilic than that of CNT-HCl (74°) and CNT-HNO_3 (70 °), and it attributes to more defects sites of CNT-EO surface which were proven by SEM and Raman. Another important properties of CNT, the surface area, were measured, and the surface area of CNT-EO (120.7 m^2/g) is near equal to that of CNT-HNO3 (122.1), but is the half of that of CNT-HCl (255.8) (see Table S1 in SI).

3.2 CNT Anodic Performance as a Function of Specific Surface Functional Group

The anodic CNT phenol TOC removal over 180 minutes of electrochemical filtration at an anode potential of 1.6 V as a function of specific CNT is presented in Figure 3A (Time-dependent phenol degradation is listed in figure S3) ; J = 1.6 mL min^{-1}, [PhOH] = 1.0 mM, and [Na_2SO_4] = 100 mM. The CNT-EO removed 0.22±0.02 mg C h^{-1} cm^{-2}, nearly 2-fold greater than the fresh-CNT at 0.12±0.02 mg C h^{-1} cm^{-2}, and nearly 4-fold greater than the CNT-HNO_3 sample at 0.06±0.01 mg C h^{-1} cm^{-2}. The oxalate TOC removal over 180 minutes at an anode potential of 2.3 V as a function of specific CNT is presented in Figure 3B; J = 1.6 mL min^{-1}, [Oxalate] = 5.0 mM, and [Na_2SO_4] = 100 mM. The relative oxalate removal has a similar trend to phenol in regards to anode material: CNT-EO (0.48 mg C h^{-1} cm^{-2}) > fresh-CNT (0.35 mg C h^{-1} cm^{-2}) > CNT-HNO_3 (0.24 mg C h^{-1} cm^{-2}). For both phenol and oxalate, the oxidative flux increases with the increasing surface hydroxyl content (or decreasing surface carboxylate content) of the CNT sample.

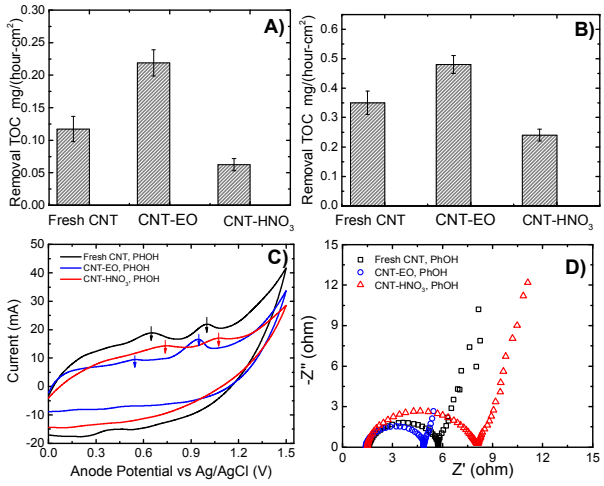

Figure 3. Anodic performance evaluation of the CNT samples. Electrochemical conditions were J = 1.6 mL min-1, [PhOH] = 1.0 mM, and [Na_2SO_4] = 100 mM unless otherwise noted. **A)** average TOC removal rate over 180 minutes of continued electrochemical filtration at an anode potential of 1.6 V; **B)** average TOC removal rate of 5 mM oxalate at anode potential 2.3V, other conditions same as **A)**; **C)** CV of phenol with a scan rate of 10 mV s-1, **D)**. EIS was measured with a three-electrode system over a frequency range of 0.1-10^6 Hz. The fresh-CNT sample is black, the CNT-EO sample is blue, and the CNT-HNO_3 sample is red in **C)** and **D)**.

To support the electrooxidative flux results, CV and EIS were completed during electrochemical filtration of phenol and the results are presented in Figure 3C and 2D, respectively, (conditions similar to Figure 3A) for the fresh-CNT (black), CNT-EO (blue), and CNT-HNO_3 (red). In all CV, The most predominant peak of phenol oxidation followed the order: CNT-HNO_3 (1.075 V) > fresh-CNTs (0.972 V) > CNT-EO (0.942 V). The CV results are in agreement with the phenol electrooxidative flux results as the lowest phenol electrooxidation overpotential is observed for the CNT-EO and the highest for CNT-HNO_3. The one-electron oxidation of phenol, eq. 1, has a standard oxidation potential of 0.63 V [37].

$$C_6H_5OH \rightarrow C_6H_5O\bullet + e^- + H^+; \quad E^0 = 0.63 \text{ V (vs Ag/AgCl)} \quad (1)$$

The continued electrochemical oxidation of the phenol radical in eq. 1 would first result in the formation of hydroquinones ($C_6H_4(OH)_2$) and benzoquinones ($C_6H_4O_2$), which could be further oxidized to small organic acids (maleic, formic, oxalic acid), and finally mineralized to carbon dioxide and water at high anode potentials [38]. If the anode potential is not great enough, the intermediate phenolic free-radicals adsorbed to the CNT network surface may polymerize with other adsorbed phenols via a radical chain mechanism [38-40], and the above-mentioned intermediates of phenol electro-oxidation were also detected by UPLC-MS (see Figure S4).

The EIS are also in agreement with the electrooxidative flux and CV results. The charge transfer resistance follows the order: CNT-EO (3.27 Ω) < fresh-CNT (4.13 Ω) < CNT-HNO_3 (6.50 Ω). The order of charge transfer resistance again indicates that CNT surface hydroxyl groups result in an acceleration of electron transfer rate. Previous studies have indicated that the edge-plane-like graphitic defect sites such as surface oxy-groups are the predominant electron transfer sites. [24-26] A notable difference between a CNT surface hydroxyl and carboxylate group is that the formation of the former does not require C-C bond-breaking whereas the latter necessitates C-C bond-breaking. A C-C bond-breaking process will have significant effects on CNT electrical properties.[41]

3.3 Ferricyanide and Ascorbate Electrooxidative Flux as a Function of CNT Functional Group

Ferrocyanide ($[Fe(CN)_6]^{4-/3-}$) is a classic anodic molecular probe as it is undergoes an ideal outer-sphere electron transfer and has negligible adsorption [28, 42]. Flow-through CV was completed for the fresh-CNT (black), CNT-EO (blue), and CNT-HNO_3 (red) at a scan rate of 10 mV s^{-1} using $[Fe(CN)_6]^{4-}$ = 1 mM with flow rate 1.6 ml min^{-1} as displayed in Figure 4A.

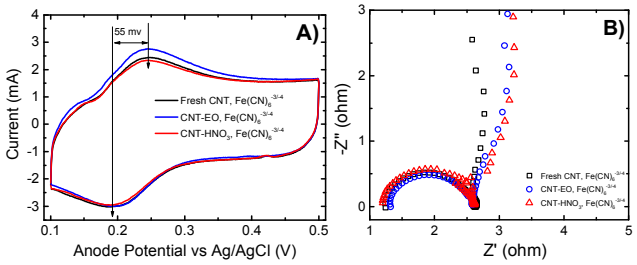

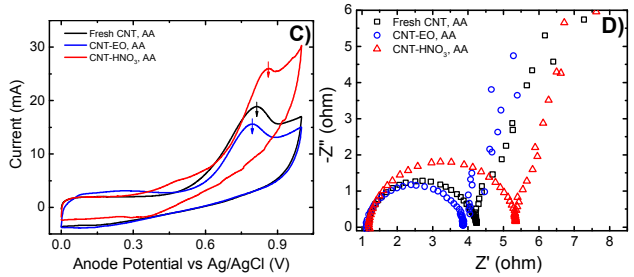

Figure 4. CV and EIS of $K_3Fe(CN)_6$ and ascorbic acid. Electrochemical conditions were J = 1.6 mL min-1, [model indicator] = 1.0 mM, and [Na_2SO_4] = 100 mM unless otherwise noted. In all cases, the fresh CNT are in black, the CNT-EO is in blue, and the CNT-HNO_3 is in red. **A)** and **C)** are CV with a scan rate of 10 mV s^{-1} of $K_3Fe(CN)_6$ and ascorbic acid(AA), respectively, **B)** and **D)** are EIS of $K_3Fe(CN)_6$ and ascorbic acid(AA), respectively, which was measured with a three-electrode system over a frequency range of 0.1-10^6 Hz.

For all CNT, the CV are quite similar and the peak-to-peak separation (ΔE_p) was ~55 mV lesser than 59 mV that is indicative of an ideal one-electron Nernst system with diffusion control due to convective mass transfer enhancements. The CV results are supported by the EIS data as presented in Figure 4B. For all CNT, the charge transfer resistance is quite similar at fresh-CNT (1.38 Ω) ~ CNT-EO (1.31 Ω) ~ CNT-HNO_3 (1.41 Ω). The similar $[Fe(CN)_6]^{4-/3-}$ redox peak positions and charge transfer resistances of the three CNT samples suggests that since $[Fe(CN)_6]^{4-/3-}$ oxidation is an outer-sphere reaction and the specific surface groups are of no consequence. This is in agreement with previous studies that have reported that $[Fe(CN)_6]^{4-/3-}$ redox reactions occur predominantly at the CNT sidewalls.[43]

Ascorbic acid (AA) is another common electrochemical probe that is oxidized through an inner-sphere electron-transfer mechanism and whose electron-transfer kinetics are highly sensitive to the properties of the electrode surface such as the electronic state and surface functional groups [28, 42]. Flow-through CV was completed for the fresh-CNT (black), CNT-EO (blue), and CNT-HNO_3 (red) at a scan rate of 10 mV s^{-1} using [AA] = 1 mM with flow rate 1.6 ml min^{-1} and are presented in Figure 4C.

The oxidation peak potentials ($E_{p,a}$) follow the order: CNT-EO (0.79 V) < fresh-CNT (0.81 V) < CNT-HNO_3 (0.86 V) similar to the phenol oxidation potential order, but of lesser magnitude. In agreement with the CV data, the EIS for the three CNT is presented in Figure 4D (and Table 2) and follow the order: CNT-EO (2.74 Ω) < fresh-CNT (3.05 Ω) < CNT-HNO_3 (4.17 Ω).

Table 2. Summary of the oxidation and reduction peak potentials and EIS. Ep,a , Ep,c is anode and cathode peak potential, respectively

	$E_{p,a}$ (V)			$E_{p,a}$ - $E_{p,c}$ (V)			EIS (Ω)		
	CNT-EO	CNT	CNT-HNO_3	CNT-EO	CNT	CNT-HNO_3	CNT-EO	CNT	CNT-HNO_3
$Fe(CN)_6^{-3/-4}$	0.245	0.245	0.245	0.055	0.054	0.054	1.31	1.38	1.41
AA	0.792	0.812	0.864	N/A	N/A	N/A	2.74	3.05	4.17
Phenol	0.942	0.972	1.075	N/A	N/A	N/A	3.27	4.13	6.50

In summary, the three inner-sphere electron transfer probes; phenol, oxalate, and ascorbate, are all observed to have specific CNT surface defect oxy-group dependent kinetics where surface hydroxyl groups tend to increase kinetics and surface carboxylate groups tend to decrease kinetics. The outer-sphere electron transfer probe, ferrocyanide, is observed to have kinetics independent of specific CNT surface oxy-group suggesting electron transfer is predominantly through the CNT sidewalls. [43, 44]

3.4 Phenol Oxidation Mechanism as a Function of CNT Surface Groups

The specific advanced oxidation process can oxidize CNT via a range of oxidants and mechanisms i.e., thermal HNO_3 (NO_2^+) versus electrochemical persulfate or sulfate radical (SO_4^{2-} + 2 h^+ → $S_2O_8^{2-}$; SO_4^{2-} + h^+ → $SO_4^{\cdot-}$) [45], and in turn the specific CNT surface groups may be different. Similar to observations here, recent studies have found that CNT treated with HNO_3 yielded a greater fraction of surficial carboxyl groups (-COOH) and CNT treated with persulfate from electrochemical process yielded a greater fraction of surficial hydroxyl groups (-COH) [36, 46]. Here, we also observed the specific CNT surface group also effects inner sphere electrooxidation kinetics. For example, the CNT-EO with increased -COH surface groups had greater phenol, oxalate, and AA electrooxidation kinetics than the CNT-HNO_3 that predominantly (>95% surface groups) –COOH surface groups. One hypothesis for the surface group dependent electrooxidation kinetics is that the different CNT surface groups may also have different oxidation strengths and pathways, e.g., and plausible surface reaction mechanisms eq. 2 & 3 for carboxyl and eq. 4 for hydroxyl.

$$\text{CNT—COO-} + h+ \rightarrow \text{CNT—COO}\bullet \rightarrow \text{CNT}\bullet + CO_2 \quad (2)$$

$$\text{CNT}\bullet + O_2 \rightarrow \text{CNT-OO}\bullet \quad (3)$$

$$\text{CNT—OH(H-O-H)} + h+ \rightarrow \text{CNT—OH} + \text{HO}\bullet \quad (4)$$

The one-electron oxidation of a surface carboxyl group will result in immediate decarboxylation and the formation of a weakly oxidizing carbon radical, eq. 2, that will react at diffusion controlled rates with O_2 forming a peroxy radical, eq. 3, which in turn may lead to a radical chain. In contrast, the oxidation of a hydroxyl group will yield a surface-bound hydroxyl radical, one of the strongest oxidants known. To examine the potential of each CNT for electrochemical HO· generation, 1 mM salicylic acid was used as a HO· trapping agent, eq. 5, via formation of dihydroxybenzoic acids (dHBA).

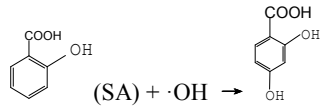

(SA) + ·OH → (5)

Salicylic acid and its primary aqueous oxidation products were quantified and verified via HPLC-fluorescence and UPLC-MS, respectively, as displayed in Figure 5.

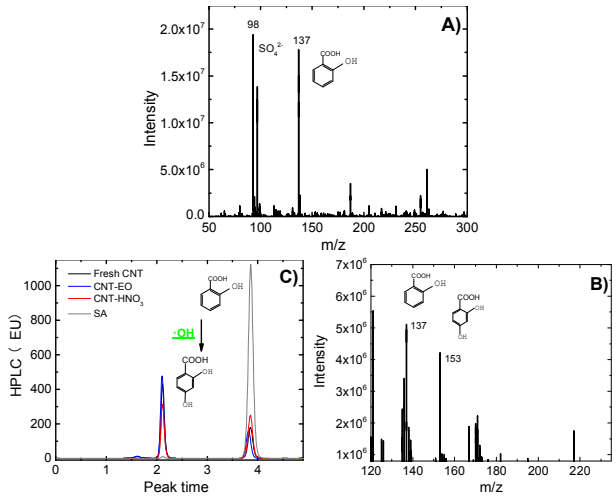

Figure 5. Detection of hydroxyl radical in electrochemical oxidation process by HPLC and identication by UPLC-MS. 1mM SA in 10 mM Na_2SO_4, as the trap agent of hydroxyl radical, flows through the electrochemical filters under 3 V, and **A)** the MS of 1mM SA in 10 mM Na_2SO_4, the intermediates of SA reaction with hydroxyl radical were detected and verified by UPLC-MS **B)**, and via HPLC **C)**.

Interestingly, the yields of dHBA (m/z = -153) i.e., HO·, for the three CNT follows the order: CNT-EO > fresh-CNT > CNT-HNO_3, which are consistent with electrochemical degradation rates of phenol and oxalate on three kinds of CNT filters. Obviously, CNT via anodic oxidation (CNT-EO) produce more ·OH which is responsible for its higher electrochemical performance.

Another consequent concern is why CNT-EO with more –COH surface group can produce more ·OH, and this attributes possibly to the below aspects. 1) The CNT-EO contains more -COH and thus electron-transfer sites since -COH can produce two times defects sites of -COOH under similar O/C ratio basing on that -COH only contains one oxygen atom per carbon and -COOH contains two oxygen atoms per carbon, and this imagination were supported by TEM and SEM and Raman results which proven there were more defects sites or active sites on CNT-EO. 2) C-OH on CNT are more hydrophilic than COOH, which were supported by the measurement of contact angle in Figure 2, and it's due to formed H-bond with H_2O (C-O···H-O-H) and C-OH, furthermore, H_2O plays the most important role in indirect electrooxidation process and nearly all intermediate oxidants (containing ·OH, H_2O_2 and O^{2-}· etc.) derive from H_2O followed the below steps from eq.6 to eq.9.

CNT-OH + H_2O → CNT-HO···H-O-H (adsorption et al.) (6)

CNT-HO···H-O-H → CNT-OH(·OH) + e^- + H^+ (·OH production in anode) (7)

CNT-OH(·OH) → CNT-OH + **·OH** (release of ·OH into aqueous solution) (8)

·OH + P (Pollutants, SA) >> CO_2 + H_2O (·OH oxidizes pollutants) (9)

Thus, more surface H_2O on CNT-EO due to more defect sites and hydrophilic properties mean more electron-transfer sites and reaction chances, which are responsible for its admirable anodic performance. Actually, EIS data in figure 3D and 4D, which

represent the faradic electron transfer rate in electrochemical reaction, indicate that CNT-EO shows the lowest reaction resistance and the fast electron transfer rate, and this agree well with the above analysis.

4. Conclusions

Anode materials will be oxidized inevitably during electrochemical applications under high anode potential, which is a major concern as it degrades sharply anode performance [11-15]. However, the observation that CNT electrooxidation results in enhanced anodic performance due to the formed -COH may change the paradigm that anode corrosion is a negative process. When pure CNT anodes are utilized, electrooxidation of CNT is seen to enhance rather than reduce key properties, and the operator will not have to worry about loss of electrochemical activity due to the electrooxidation. This is a quite important guidance for CNT anodes application in wastewater treatment field where high anode potentials (> 2 V) may be necessary to completely mineralize recalcitrant pollutants to carbon dioxide for complete removal of TOC, one of the most important indices in wastewater treatment. And the above findings may guide researchers to realize the potential of using CNT anodes as well as the importance of specific CNT surface functionalities on electrochemical processes that may excite more researches in the area.

Acknowledgments

G.G. thanks the Chinese Scholarship Council (CSC) and Harvard Graduate School of Arts and Sciences (GSAS) Visiting Fellow Scholarship and Key Project of Chinese National Programs for Fundamental Research and Development (973 Program) (NO: 2014CB932001). We thank Harvard's Center for Nanoscale Systems for SEM. We thank the Korean Institute of Geosciences and Mineral Resources for funding (NO: 214551-01).

Notes and references

[a] Key Laboratory of Pollution Processes and Environmental Criteria (Ministry of Education) / Tianjin Key Laboratory of Environmental Remediation and Pollution Control, College of Environmental Science and Engineering, Nankai University, Tianjin 300071, China
[b] School of Engineering and Applied Sciences, Harvard University, Cambridge, MA 02138
*Corresponding author, Guandao Gao, Tel/Fax: +0086-22-23501117, E-mail: Gaoguandao@nankai.edu.cn

Electronic Supplementary Information (ESI) available: Images of the electrochemical filtration apparatus (S1) and Images of a representative CNT network (S2) etc. are available free of charge via the Internet. See DOI: 10.1039/b000000x/

1. J. Gonzalez-Garcia, V. Montiel, A. Aldaz, J. A. Conesa, J. R. Perez and G. Codina, *Ind. Eng. Chem. Res.*, 1998, **37**, 4501-4511.
2. J. Gonzalez-Garcia, P. Bonete, E. Exposito, V. Montiel, A. Aldaz and R. Torregrosa-Macia, *J. Mater. Chem.*, 1999, **9**, 419-426.
3. J. Yang, D. W. Hand, D. R. Hokanson and J. C. Crittenden, *Environmental Science & Technology*, 2002, **37**, 428-436.
4. Z. Shen, J. Yang, X. Hu, Y. Lei, X. Ji, J. Jia and W. Wang, *Environmental Science & Technology*, 2005, **39**, 1819-1826.
5. E. Kjeang, R. Michel, D. A. Harrington, N. Djilali and D. Sinton, *Journal of the American Chemical Society*, 2008, **130**, 4000-4006.
6. J. Yang, J. Wang and J. Jia, *Environmental Science & Technology*, 2009, **43**, 3796-3802.
7. D. Tasis, N. Tagmatarchis, A. Bianco and M. Prato, *Chem. Rev.*, 2006, **106**, 1105-1136.
8. K. A. Wepasnick, B. A. Smith, J. L. Bitter and D. H. Fairbrother, *Analytical and Bioanalytical Chemistry*, 2010, **396**, 1003-1014.
9. G. Gao and C. D. Vecitis, *Environmental Science & Technology*, 2011, **45**, 9726-9734.
10. C. D. Vecitis, M. H. Schnoor, M. S. Rahaman, J. D. Schiffman and M. Elimelech, *Environmental Science & Technology*, 2011, **45**, 3672-3679.
11. Y. Shao, G. Yin, J. Zhang and Y. Gao, *Electrochimica Acta*, 2006, **51**, 5853-5857.
12. H. Wu, D. Wexler and H. Liu, *Journal of Solid State Electrochemistry*, 2011, **15**, 1057-1062.
13. R. Berenguer, J. P. Marco-Lozar, C. Quijada, D. Cazorla-Amoros and E. Morallon, *Carbon*, 2012, **50**, 1123-1134.
14. C. U. Pittman, W. Jiang, Z. R. Yue, S. Gardner, L. Wang, H. Toghiani and C. Leon, *Carbon*, 1999, **37**, 1797-1807.
15. Z. R. Yue, W. Jiang, L. Wang, S. D. Gardner and C. U. Pittman, *Carbon*, 1999, **37**, 1785-1796.
16. A. Rauscher, G. Kutsan and Z. Lukacs, *Corrosion Science*, 1990, **31**, 255-260.
17. C. Dafonseca, S. Boudin and M. D. Belo, *Journal of Electroanalytical Chemistry*, 1994, **379**, 173-180.
18. E. J. Kelly, *Journal of the Electrochemical Society*, 1979, **126**, 2064-2075.
19. R. E. Hummel, R. J. Smith and E. D. Verink, *Corrosion Science*, 1987, **27**, 803-813.
20. D. Sazou, M. Pagitsas and C. Georgolios, *Electrochimica Acta*, 1992, **37**, 2067-2076.
21. J. J. Gooding, *Electrochimica Acta*, 2005, **50**, 3049-3060.
22. J. J. Gooding, R. Wibowo, J. Q. Liu, W. R. Yang, D. Losic, S. Orbons, F. J. Mearns, J. G. Shapter and D. B. Hibbert, *Journal of the American Chemical Society*, 2003, **125**, 9006-9007.
23. K. Hata, D. N. Futaba, K. Mizuno, T. Namai, M. Yumura and S. Iijima, *Science*, 2004, **306**, 1362-1364.
24. C. E. Banks, T. J. Davies, G. G. Wildgoose and R. G. Compton, *Chem. Commun.*, 2005, 829-841.
25. C. E. Banks, R. R. Moore, T. J. Davies and R. G. Compton, *Chem. Commun.*, 2004, 1804-1805.
26. A. Chou, T. Bocking, N. K. Singh and J. J. Gooding, *Chem. Commun.*, 2005, 842-844.
27. I. Heller, J. Kong, H. A. Heering, K. A. Williams, S. G. Lemay and C. Dekker, *Nano Lett.*, 2005, **5**, 137-142.
28. K. P. Gong, S. Chakrabarti and L. M. Dai, *Angewandte Chemie International Edition*, 2008, **47**, 5446-5450.
29. I. Dumitrescu, P. V. Dudin, J. P. Edgeworth, J. V. Macpherson and P. R. Unwin, *The Journal of Physical Chemistry C*, 2010, **114**, 2633-2639.
30. H. P. Boehm, E. Diehl, W. Heck and R. Sappok, *Angewandte Chemie International Edition in English*, 1964, **3**, 669-677.
31. J. Jen, M.-F. Leu and T. C. Yang, *Journal of chromatography A*, 1998, **796**, 283-288.
32. J. Shen, A. Liu, Y. Tu, G. Foo, C. Yeo, M. B. Chan-Park, R. Jiang and Y. Chen, *Energy & Environmental Science*, 2011, **4**, 4220-4229.
33. S.-C. Wang, J. Yang, X.-Y. Zhou and J. Xie, *Electronic Materials Letters*, 2014, **10**, 241-245.
34. M. Seredych, D. Hulicova-Jurcakova, G. Q. Lu and T. J. Bandosz, *Carbon*, 2008, **46**, 1475-1488.
35. P. Chingombe, B. Saha and R. Wakeman, *Carbon*, 2005, **43**, 3132-3143.
36. V. Datsyuk, M. Kalyva, K. Papagelis, J. Parthenios, D. Tasis, A. Siokou, I. Kallitsis and C. Galiotis, *Carbon*, 2008, **46**, 833-840.
37. P. Wardman, *J. Phys. Chem. Ref. Data*, 1989, **18**, 1637-1755.
38. C. Comninellis and C. Pulgarin, *Journal of Applied Electrochemistry*, 1993, **23**, 108-112.
39. T. A. Enache and A. M. Oliveira-Brett, *Journal of Electroanalytical Chemistry*, 2011, **655**, 9-16.
40. N. B. Tahar and A. Savall, *Journal of the Electrochemical Society*, 1998, **145**, 3427-3434.

41. M. Dresselhaus, G. Dresselhaus, J.-C. Charlier and E. Hernandez, *Philosophical Transactions of the Royal Society of London. Series A: Mathematical, Physical and Engineering Sciences*, 2004, **362**, 2065-2098.
42. R. L. McCreery, *Chem. Rev.*, 2008, **108**, 2646-2687.
43. I. Dumitrescu, P. R. Unwin and J. V. Macpherson, *Chemical Communications*, 2009, 6886-6901.
44. K. Gong, S. Chakrabarti and L. Dai, *Angewandte Chemie-International Edition*, 2008, **47**, 5446-5450.
45. H. Park, C. D. Vecitis and M. R. Hoffmann, *The Journal of Physical Chemistry C*, 2009, **113**, 7935-7945.
46. K. A. Wepasnick, B. A. Smith, K. E. Schrote, H. K. Wilson, S. R. Diegelmann and D. H. Fairbrother, *Carbon*, 2011, **49**, 24-36.

Graphical abstract: